Osteoarthritis and Cartilage 27 (2019) 1841–1850

Osteoarthritis and Cartilage

OARSI OSTEOARTHRITIS RESEARCH SOCIETY INTERNATIONAL

Real-time optical redox imaging of cartilage metabolic response to mechanical loading

S.K. Walsh †, M.C. Skala ‡ §, C.R. Henak § || ¶ *

† Comparative Biomedical Sciences Program, University of Wisconsin–Madison, Madison, WI, USA
‡ Morgridge Institute for Research, Madison, WI, USA
§ Department of Biomedical Engineering, University of Wisconsin–Madison, Madison, WI, USA
|| Department of Mechanical Engineering, University of Wisconsin–Madison, Madison, WI, USA
¶ Department of Orthopedics and Rehabilitation, University of Wisconsin–Madison, Madison, WI, USA

ARTICLE INFO

Article history:
Received 1 March 2019
Accepted 29 August 2019

Keywords:
Articular cartilage
Metabolism
Glycolysis
Oxidative phosphorylation
Redox
Mechanical loading

SUMMARY

Objective: Metabolic dysregulation has recently been identified as a key feature of osteoarthritis. Mechanical overloading has been postulated as a primary cause of this metabolic response. Current methods of real-time metabolic activity analysis in cartilage are limited and challenging. However, optical redox imaging leverages the autofluorescence of co-enzymes NAD(P)H and FAD to provide dye-free real-time analysis of metabolic activity. This technique has not yet been applied to cartilage. This study aimed to assess the effects of a compressive load on cartilage using optical redox imaging.
Method: Cartilage samples were excised from porcine femoral condyles. To validate this imaging modality in cartilage, glycolysis was inhibited via 2-deoxy-D-glucose (2DG) and oxidative phosphorylation was inhibited by rotenone. Optical redox images were collected pre- and post-inhibition. To assess the effects of mechanical loading, samples were subjected to a compressive load and imaged for approximately 30 min. Load and strain parameters were determined using high-speed camera images in Matlab. A range of loading magnitudes and rates were applied across samples.
Results: 2DG and rotenone demonstrated the expected inhibitory effects on fluorescence intensity in the channels corresponding to NAD(P)H and FAD, respectively. Mechanical loading induced an increase in NAD(P)H channel fluorescence which subsided by 30 min post-loading. Magnitude of loading parameters had mixed effects on metabolites.
Conclusions: Optical redox imaging provides an opportunity to assess real-time metabolic activity in cartilage. This approach revealed a metabolic response to a single load and can be used to provide insight into the role of metabolism in mechanically-mediated cartilage degradation.

Introduction

Metabolic dysregulation occurs in many diseases and has recently been implicated as a feature of mechanically-mediated articular cartilage damage. Broadly, metabolism serves to generate energy in the form of adenosine triphosphate (ATP) via glycolysis, which occurs in the cytosol, and oxidative phosphorylation, which occurs in the mitochondria[1]. A shift in metabolic balance between energetic reliance on glycolysis and oxidative phosphorylation, respectively, can occur in disease states as a maladaptive response, or as a return to a more embryonic phenotype. For example, the Warburg effect is a well-established marker of cancer phenotype[2]. The resulting upregulation of glycolysis results either from mitochondrial dysfunction or from demand for secondary products required for cellular proliferation and extracellular matrix formation[3]. Compared to healthy articular cartilage, growth plate cartilage exhibits a Warburg-like metabolic phenotype, with greater relative reliance on glycolysis[1,4]. Osteoarthritic cartilage has been shown to revert to a metabolic phenotype similar to that of the growth plate, demonstrating greater relative glycolytic activity and lower oxidative phosphorylation activity than healthy articular cartilage[1,5,6]. Recent evidence suggests

* Address correspondence and reprint requests to: C.R. Henak, Department of Biomedical Engineering, University of Wisconsin–Madison, 3031 Mechanical Engineering Building, 1513 University Ave, Madison, WI, 53706, USA. Tel: 608-263-1619.
E-mail address: chenak@wisc.edu (C.R. Henak).

https://doi.org/10.1016/j.joca.2019.08.004
1063-4584/

articular cartilage metabolism is also altered in response to mechanical load, with extreme cases leading to tissue damage via multiple mechanisms. Superphysiological loading alters basal and maximal respiration, repetitive cyclic loading exacerbates stress-dependent metabolic dysfunction, and mitochondrial damage precedes osteoarthritis-like macroscopic cartilage damage[7–9]. Additionally, non-pathway-specific metabolic activity has shown sensitivity to mechanical loading, including changes over less than 1 h after superphysiological loading[10–15]. Despite this body of associative evidence, the role of short term mechanically-mediated metabolic flux, defined here as a detectable increase or decrease in metabolic activity, in long term metabolic dysregulation and cartilage degradation remain unclear. This is in part due to limited methods established for nondestructively evaluating short-term metabolic flux in cartilage.

There are several established techniques for evaluating metabolism in cartilage. Metabolic biomarkers and regulatory factors associated with cartilage damage have been identified by qPCR, mass spectrometry, and RNA sequencing[16–18]. Computational modeling has been combined with experimental metabolomic data to predict metabolic response to dynamic loading on the cellular level[19]. Commercially available kits have allowed for functional analysis of mitochondria, including respiration, depolarization, and ROS release[8,9,20,21]. Intracellular calcium flux has been imaged in real-time under axial compression to indicate immediate metabolic response to mechanotransduction[10,11,22]. Though informative, these techniques are limited to single time points, exogenous dyes, non-specific evaluation, or sample-destructive methods. Thus, non-destructive methods capable of longitudinally analyzing specific metabolic activity in cartilage tissue have not been established.

Conversely, a real-time imaging technique for evaluation of relative oxidative phosphorylation and glycolysis activity has been established for other tissues[23–25]. Optical redox imaging leverages the autofluorescence of flavin adenine dinucleotide (FAD) and nicotinamide adenine dinucleotide (NADH), which are electron acceptors and donors, respectively, in an array of metabolic reactions. Fluorescence intensity of each metabolite is correlated with its concentration. Intensity changes in the fluorescence channels corresponding to these respective metabolites can be interpreted as congruous changes in the accumulation of these metabolites, and, thus, altered activity of the metabolic processes that created them[23,26]. Additionally, optical redox ratio, a measure of the oxidative-reduction status of the mitochondrial matrix, can be calculated from the fluorescence intensities of FAD and NADH, and changes in optical redox ratio can be interpreted as changes in relative activity levels of mitochondrial and nonmitochondrial metabolic activity, respectively. It should be noted that fluorescence properties of NADH are identical to nicotinamide adenine dinucleotide phosphate (NADPH), so the fluorescence in this channel includes a contribution from both metabolites. The combined fluorescence is denoted as NAD(P)H.

Optical redox imaging has been employed in cancer and stem cell research, and is sensitive to relative changes in glycolysis and oxidative phosphorylation, but has not yet been applied to cartilage[23,24,27–30]. However, previous studies have directly and indirectly measured activity of glycolysis and oxidative phosphorylation in cartilage via alternative techniques, reporting metabolic flux as a notable feature of disease and mechanotransduction[12,31–34]. This line of research would benefit substantially from development of a label-free, nondestructive technique capable of detecting time- and mechanical load-dependent shifts in metabolic activity of whole tissue explants. Therefore, the objectives of this study were to validate real-time optical redox imaging in articular cartilage, then to use this method to detect metabolic flux in response to a single compressive load.

Methods

Sample collection & preparation

Cartilage samples were collected from femoral condyles of 5-6-month-old pigs at a local abattoir within 6 h of sacrifice. Full-thickness cylindrical plugs were excised using a 4 mm diameter biopsy punch and scalpel. Samples were stored in chondrocyte media containing Ham's F-12 media (Mediatech, Inc., Manassas, VA), 10% fetal bovine serum (Hyclone, GE Healthcare Bio-Sciences, Pittsburgh, PA), 50 ug/ml ascorbic acid (Amresco, LLC., Solon, OH), 30 ug/ml alpha-ketoglutaric acid (Thermo Fisher Scientific Chemicals, Inc., Waltham, MA), 300 ug/ml L-glutamine, 100 IU/ml penicillin G, 100 ug/ml streptomycin, and 6 mg/ml HEPES buffer (Corning, Inc., Corning, NY) at room temperature for same-day use, or otherwise incubated at 37 °C and 5% CO_2 for up to 6 days. Days spent in culture did not affect baseline metabolic values. Subchondral bone was removed with a razor blade to create a deep surface parallel to the articular surface. Cylindrical plugs were then bisected into hemicylinders for imaging.

Metabolic imaging

Metabolic imaging was performed on an inverted epifluorescent microscope (Olympus IX-71, Tokyo, Japan) with a metal halide fluorescent lamp (X-Cite 120 Fluorescence Illumination System, Exfo Inc., Quebec, Canada). A DAPI filter cube (excitation 361–389 nm, emission 435–485 nm) was used to measure fluorescence in channel 1, in which NAD(P)H fluoresces (160–250 ms exposure time) [Fig. 1(D)], and a green filter cube (excitation 470–490 nm, emission 500–550 nm) was used to measure fluorescence in channel 2, in which FAD fluoresces (1.5–6 s exposure time) [Fig. 1(E)]. All images were captured at 40× using a 1.6× extender. Fluorescence intensities of channel 1 and channel 2 images were measured with a monochrome camera (DP80, Olympus, Tokyo, Japan), and ImageJ software was used to calculate the optical redox ratio, defined here as ORR = [FAD channel]/[NAD(P)H channel + FAD channel][24,35,36].

Imaging validation

To validate the sensitivity and specificity of this metabolic imaging method, samples were imaged before and after exposure to established metabolic inhibitors of oxidative phosphorylation and glycolysis [Fig. 1(A)]. 2-deoxy-D-glucose (2-DG) (Alfa Aesar, Haverhill, MA) is a glucose analog and inhibits glycolysis, while rotenone (Sigma–Aldrich, St. Louis, MO) is an inhibitor of mitochondrial complex I electron transport and downregulates oxidative phosphorylation[24,34]. Samples were imaged on a coverslip along the articular edge of the cross section. Preliminary cell viability imaging was performed on the cut surface of cartilage samples and revealed minimal cell death due to sample sectioning (data not shown). Control images were first taken in chondrocyte media at room temperature, and samples were then incubated for either 24 h in 10 mM 2-DG ($n = 8$ samples from 3 animals, 4 locations per sample) or for 30 min in 20 μM rotenone ($n = 9$ samples from 3 animals, 4 locations per sample) in chondrocyte media at 37°C prior to re-imaging baseline-paired locations at room temperature [Fig. 1(A)].

To confirm that the observed metabolic effects were caused by mechanical loading, a series of control experiments were performed. Unloaded samples were imaged 30 min apart with the intermediate imaging protocol applied to loaded samples to ensure time and fluorescent exposure were not causing the metabolic effects observed in loaded samples. Mechanical loading control data

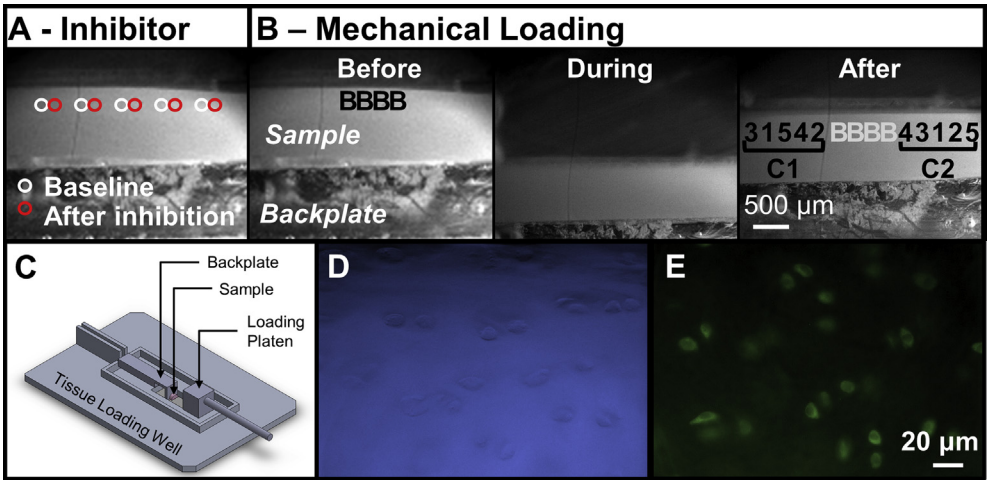

Fig. 1. Schematic overview of imaging setup. Imaging locations for chemical inhibitor validation (A) and mechanical loading (B). Imaging fields are distributed across the sample to avoid photobleaching effect. 'B' indicates the locations of baseline images, 'C1' and 'C2' indicate two clusters used for time-course analysis, and numbers indicate time post-loading bin (1 = 0–5 min, 2 = 5–10 min, 3 = 10–15 min, 4 = 15–20 min, 5 = 30–35 min). Mechanical loading tissue well (C) in which sample was submerged in PBS throughout loading and imaging. Representative metabolic images in NAD(P)H-capturing channel 1 (D) and FAD-capturing channel 2 (E). Images were captured at 40×.

showed minimal metabolic changes over time compared to loaded samples (Supplementary Fig. S1). Additionally, optical redox imaging was performed every 5 min up to 30 min on a thermal probe in place of a sample to detect temperature increase as a function of light exposure. Thermal monitoring revealed a total increase of 0.2°C from the 30 min imaging protocol applied to mechanically loaded samples (Supplementary Fig. S1).

Mechanical loading

Samples were mechanically loaded on a custom-built microscope-top loading apparatus [Fig. 1(C)]. The loading apparatus consists of a custom well and backplate that sits on top of an inverted microscope, with a custom loading platen that interfaces with an actuator (Aerotech ACT165D, Aerotech, Pittsburgh, PA). Twenty-eight samples from 10 animals were bisected into hemicylinders and adhered to a backplate on the subchondral side via cyanoacrylate with the tissue cross section flush with the imaging coverslip. While chemical inhibitor studies required submersion in chondrocyte media due to prolonged incubation, mechanical loading and subsequent imaging took place in under an hour. Thus, mechanical loading samples were submerged in PBS throughout testing and were given sufficient time to equilibrate to room temperature prior to loading and imaging. Normalization of fluorescence data to baseline intensity within each sample was assumed to account for any baseline differences in metabolism attributable to varied media between these two studies. Further, a subset of samples was subjected to the adhesion process and imaged without mechanical loading to ensure that cyanoacrylate had no significant effect on metabolism. Samples underwent a single compression using a metal platen spanning the entire articular surface; a variety of displacements and rates were applied using the actuator to achieve a range of peak strain, strain rate, force, and force rate. Mechanical loading was imaged using a high-speed camera at 100 frames per second (Phantom v1211, Vision Research, Wayne, NJ), which was sufficient to capture the displacement rates achieved. Metabolic imaging was completed pre- and post-loading. Pre-loading images were collected at the center of the sample [Fig. 1(B)]. In order to account for variation in thickness of uneven samples and resulting variation in experienced deformation, post-loading time series images were collected at randomly selected locations in two imaging clusters, one on either side of the centered baseline image cluster, up to 30 min following loading.

Metabolic image intensities were determined. For time series analysis, post-loading image intensities were normalized to average baseline fluorescence per sample. Achieved mechanical loading parameters were then determined. High-speed camera images were downsampled to 10 frames per second in Matlab (Mathworks, version R2015a). Full-thickness, 1 mm wide segments were cropped at the center location of each imaging cluster in ImageJ, and bulk compressive strain was calculated in each of these cropped sections. Custom Matlab code tracked the displacement of the platen and backplate based on image intensity[37]. Strain was calculated based on the length of the sample at each time point (distance between backplate and platen) in comparison to the length before loading began. Force was calculated based on the behavior of the backplate as a leaf spring, with a calibration constant determined by fitting an experimentally-obtained force vs displacement curve. Peak compressive strain (ε) and peak force (F) were obtained. Strain rate ($\dot{\varepsilon}$) and force rate ($\dot{F}$) were determined by fitting the segment of 30 data points immediately preceding maximum values on the strain vs time and force vs time curves, respectively, and applying a Savitzky–Golay noise-smoothing filter using open-access Matlab code[38]. In order to visualize mechanical loading time-course metabolic data comprehensively, three-dimensional plots were created in Matlab (Fig. 2, Supplementary Fig. S2 and corresponding mp4 files)[39].

Statistical analysis

Validation and mechanical loading data were not normally distributed and were therefore analyzed nonparametrically in R software (version 3.2.5). Pre- and post-inhibitor validation data were compared via paired Wilcoxon rank-sum tests.

Post-loading time and mechanical loading parameters were binned to statistically test for interactions between these covariates beyond individual regressions. Time post-loading was binned into five groups, and mechanical loading parameters (peak strain, peak force, peak strain rate, and peak force rate) were each binned into three groups: low, medium, and high loading magnitude. Mechanical bin intervals were chosen to yield comparable n-values between bins. A two-way aligned rank transformation analysis of variance (ART ANOVA) was used to assess the effects of loading

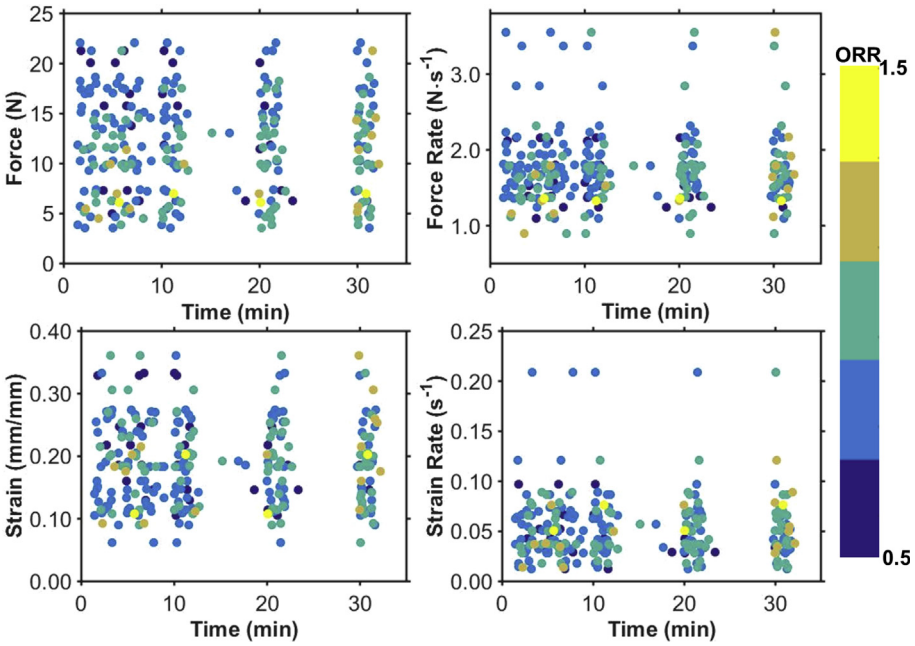

Fig. 2. Optical redox ratio as a function of time and mechanical load. Qualitative trends with time and loading are visible. Full three-dimensional results are available in the supplementary data.

parameter magnitudes and time post-loading, both main effects and the interaction, on each respective metabolic output (channel 1, channel 2, and redox ratio). Significant factors from each ANOVA were analyzed post-hoc via Tukey Honest Significant Difference (HSD) pairwise comparisons for detection of differences between binned groups.

Results

Inhibitors caused the expected changes in channels 1 and 2, validating the use of this imaging method for cartilage (Fig. 3). 2-DG, a glucose analog intended to inhibit glycolysis, decreased channel 1 (NAD(P)H) fluorescence (−13.0%) as expected, and increased channel 2 (FAD) fluorescence (+31.8%) and optical redox ratio ([FAD]/[FAD + NAD(P)H]) (+51.2%). Rotenone, an oxidative phosphorylation complex I inhibitor, caused the expected decrease of channel 2 fluorescence (−16.0%) as well as optical redox ratio (−5.4%), and also decreased channel 1 fluorescence (−5.4%). Wilcoxon rank-sum tests revealed statistically significant changes in all three metabolic outputs by both chemical inhibitors at $P < 0.05$.

A range of peak strain, force, strain rate and force rate was achieved. Peak strain ranged from 0.06 to 0.36 (average = 0.19 ± 0.07). Peak force ranged from 3.6 to 22.0N (average = 11.9 ± 5.0N). Peak strain rate ranged from 0.01 to 0.21 s^{-1} (average = 0.05 ± 0.03 s^{-1}). Peak force rate ranged from 0.90 to 3.56 $N \cdot s^{-1}$ (average = 1.75 ± 0.48 $N \cdot s^{-1}$).

Post-loading time and loading magnitude had significant independent effects on all three metabolic measurements (Figs. 4 and 5). However, none of the interactions between mechanical loading and post-loading time point were significant in the two-way ANOVAs. Channel 1 (NAD(P)H) fluorescence was consistently affected by time in all models, with an initial increase in fluorescence post-loading (+10.0% maximum) that subsided by 30 min post-loading, while channel 2 (FAD) fluorescence was unaffected by time point (Fig. 4). Peak force magnitude had significant bearing on channel 1 fluorescence, with greater force showing greater intensity (+11.2% difference maximum) (Fig. 5). Applied strain rate showed the opposite pattern, as samples subjected to high strain rate showed significantly lower channel 1 fluorescence (−5.5%) than those subjected to low strain rate (Fig. 5). However, peak strain and force rate had similar effects on channel 2 activity as on channel 1, with greater peak strain and force rate associating with greater channel 2 intensity (+6.3% and +3.7% maximum differences, respectively) (Fig. 5). Redox ratio was affected by both time and loading magnitude (Figs. 2, 4 and 5). Redox ratio was higher at later time points than earlier time points (+6.2%) (Fig. 4). Higher peak force resulted in lower redox ratio (−6.9% maximum difference), and higher strain rate resulted in higher redox ratio (+3.3% maximum difference) (Fig. 5). Statistical redox ratio trends were primarily governed by changes in channel 1 (NAD(P)H) fluorescence (Figs. 4 and 5).

Discussion

Inhibition of glycolysis and oxidative phosphorylation demonstrated the validity of using optical redox imaging to evaluate metabolic activity in articular cartilage. Although slight in magnitude, rotenone caused a decrease in channel 2 fluorescence intensity as well as redox ratio, and 2-DG caused a decrease in channel 1 fluorescence intensity and increased redox ratio. Previous studies have demonstrated similarly mild effects of these inhibitors[24,34]. The pleiotropic actions of these compounds on both metabolites of interest, though seemingly off-target, are unsurprising given the inevitable interplay between metabolic processes. For example, rotenone has demonstrated an inhibitory effect on NAD(P)H production similar to that of 2-DG[34]. Conversely, short-term NADH photobleaching has been shown to cause an immediate sharp increase in FAD fluorescence intensity, perhaps as a compensatory mechanism to maintain ATP production[40]. In cartilage, glycolysis and mitochondrial respiration have demonstrated unique coupling such that glycolytic activity relies upon reactive oxygen species generated by oxidative phosphorylation[34,41]. It is possible that the higher concentration of glycolytic inhibitor 2-DG applied in the present study than previous studies (10 mM vs 3

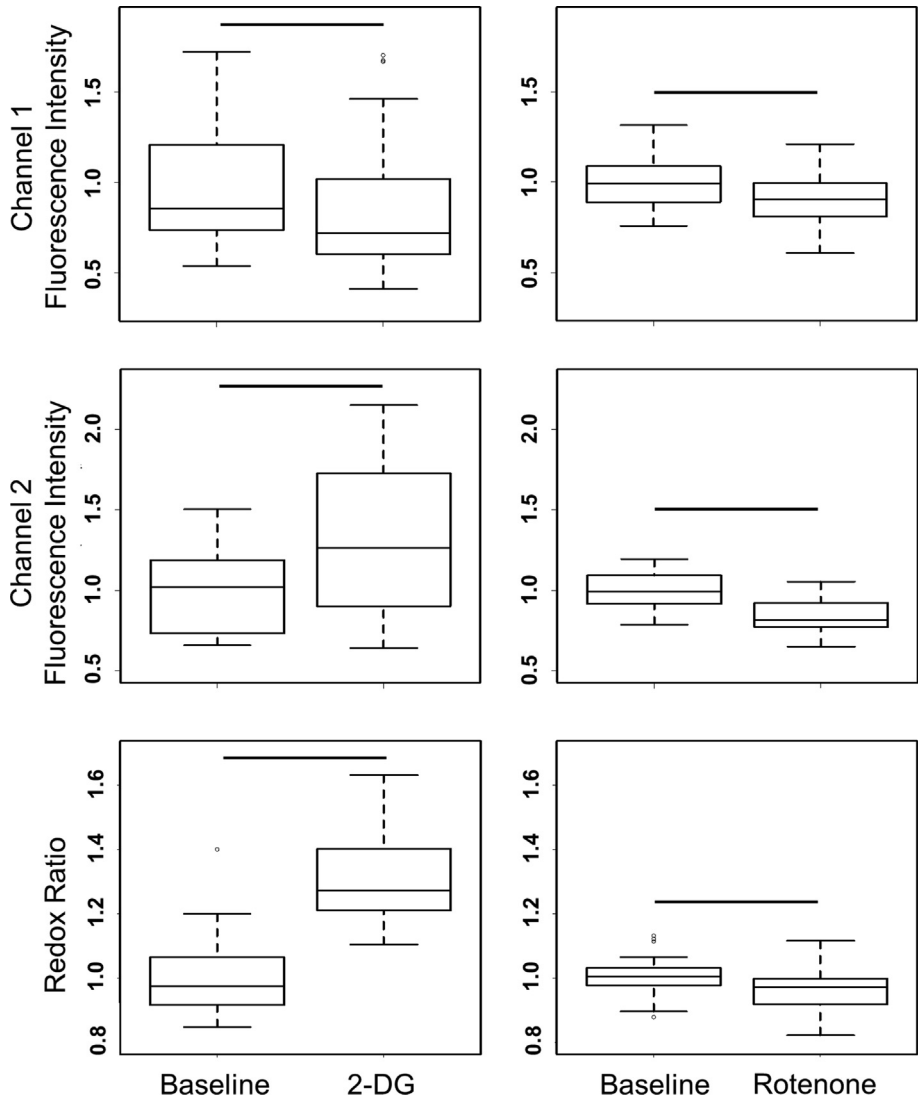

Fig. 3. Imaging results of 2-DG ($n = 32$ imaging regions from 8 samples representing 3 animals) and rotenone metabolic inhibition ($n = 36$ imaging regions from 9 samples representing 3 animals). Data are expressed as median values (lines), interquartile range (box hinges), and data range constrained to total data range multiplied by interquartile range or less (whiskers) with outliers (circles). Fluorescence intensities were normalized to average baseline values within each sample. Pre- and post-inhibitor data were compared nonparametrically via Wilcoxon rank-sum tests. Significance bars = $P \leq 0.05$.

mM) stimulated a compensatory mechanism responsible for the apparent increase in oxidative phosphorylation activity following 24-h incubation. Though the underlying mechanisms are not fully understood, the perturbation of both fluorescence channels observed from sustained chemical inhibition in the present study is ultimately not unexpected.

Metabolic imaging revealed a time-dependent response immediately following a single physiological load. The loading applied in this study was maintained below the superphysiological range, with maximum peak strain values akin to estimated strains *in vivo* during dynamic loading activities, and loading rates were several orders of magnitude below the suggested criteria for impact loading[42,43]. Increased force, strain, and force rate corresponded with increased metabolic activity. Specifically, channel 1 fluorescence was significantly increased by greater force, and channel 2 fluorescence was increased by greater strain and force rate. This is consistent with previous research showing that moderate compressive loading of healthy chondrocytes stimulates an anabolic response that increases the cells' energy requirement and necessitates an increase in metabolic activity[44,45]. Conversely, increased strain rate corresponded with significantly decreased channel 1 fluorescence and a trend of decreased channel 2 fluorescence. While these mechanical loading effects may seem contradictory, they likely arise due to rate-dependent cartilage behavior that result from poroelasticity[46,47]. Compressive strain rate is often associated with fluid flow in cartilage, which subjects chondrocytes to shear, thus inducing metabolic flux[48,49]. Though bulk strain rates in the present study were physiological, resulting in minimal fluid flow across the whole tissue, metabolic imaging evaluated a local region of cartilage just beneath a cut sample edge where fluid flow may have played a nontrivial role in the observed metabolic changes[50]. Further, additional research could clarify whether the loads applied in this study, which were highly unlikely to be injurious, could induce a healthy inhibitory effect on anabolic activity as a physiological process by which metabolic homeostasis is maintained[51,52].

Time had a significant effect on channel 1 fluorescence in all two-way ANOVAs, consistently showing greatest intensity at early

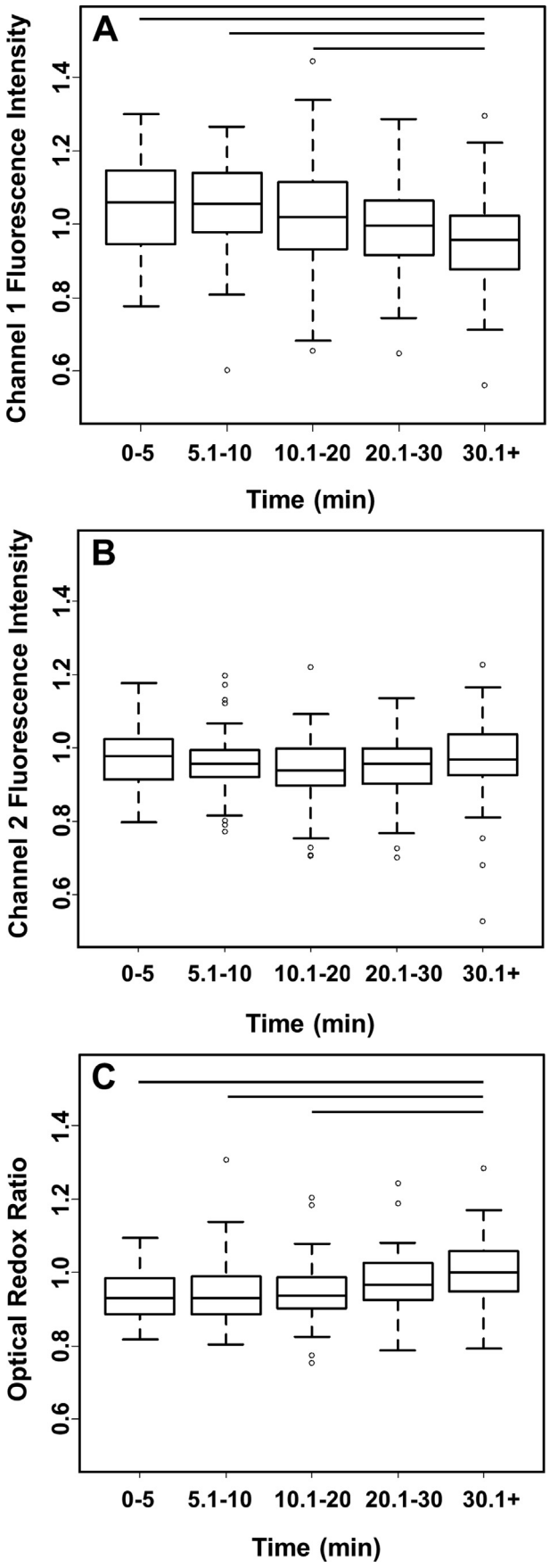

time. This result provides additional confidence that the metabolic changes observed resulted from mechanical loading, as metabolic activity induced simply by time in non-physiological conditions alone would be expected to be minimal in the early time points. The same reasoning applied to the effect of mechanical loading magnitude, wherein compression stimulates anabolism, may pertain to time effect as well, as the stimulatory response observed early after loading appears to dissipate within 30 min. The decrease in channel 1 fluorescence by 30 min provides further evidence of the mild nature of the compression and in this study and confirms that the chosen time points capture the early effects of a single load. Indeed, it is prudent that the present study results are not over-interpreted on a mechanistic level given the limitations of the metabolic analysis method employed and as well as the simplicity of the applied loading regime. Rather, the present study reveals short-term variation in metabolic response to mechanical loading, leaving future studies with additional questions and a useful tool to tease out the mechanical thresholds that result in healthy and unhealthy cartilage response.

It is worth noting that the statistical model employed was chosen to allow for two-way ANOVA using nonparametric data. This model is unable to accommodate inclusion of individual animal source as a third covariate in addition to timepoint and mechanical input. However, animal-dependent variations were of interest, as samples from the same animal are not truly independent. Therefore, using the current statistical model, two-way ANOVAs were conducted with timepoint and animal as covariates against all three metabolic outputs (channel 1, channel 2, redox ratio) with post-hoc Tukey-corrected pairwise comparisons. Channel 1 and redox ratio showed no statistically significant pairwise comparisons between animal sources and very few approaching significance, and channel 2 output showed relatively few significant differences between animal sources (at $P < 0.05$). Given the random distribution of mechanical bins, sample numbers did not allow for further two-way ANOVAs testing animal source against mechanical input as the two covariates. However, in light of the results of timepoint by animal interaction analyses and the known consistency of animal source with respect to age, breed, approximate weight, housing conditions, and macroscopic tissue health, interpreting statistical analyses in which individual animal factor is omitted was considered to be appropriate for the current study.

Given that channel 2 (FAD) showed minimal changes compared to channel 1 (NAD(P)H), it is unsurprising that redox ratio appeared to be largely governed by channel 1 trends, mirroring all findings of statistical significance of this channel. It is well known that glycolysis is a faster method of ATP production than oxidative phosphorylation[3,53]. As such, it follows that these pathways would exhibit differential sensitivity to environmental perturbations with glycolysis likely showing earlier and possibly more robust effects, and that the byproducts of these processes would reflect this discrepancy. It is also unsurprising that channel 1 and channel 2 intensities were affected in largely the same direction by all mechanical parameters. A shift in metabolic preference indicated by a lasting increase or decrease in redox ratio, as observed in osteoarthritic chondrocytes, would signal a meaningful change in biological phenotype unlikely to be incited by a single load well below suggested thresholds for mechanical injury induction[5,6,43]. It should be noted that it is possible that mechanical loading such as

Fig. 4. Metabolic outputs as a function of time. NAD(P)H fluorescence intensity is captured by channel 1 (A), FAD intensity is captured by channel 2 (B), and redox ratio (C) is calculated as [FAD]/[NAD(P)H + FAD]. Fluorescence intensities were normalized to baseline values averaged within each sample (per time bin: $n = 49–58$ images from 25 to 27 samples representing 10 animals). Significance bars = $P \leq 0.05$.

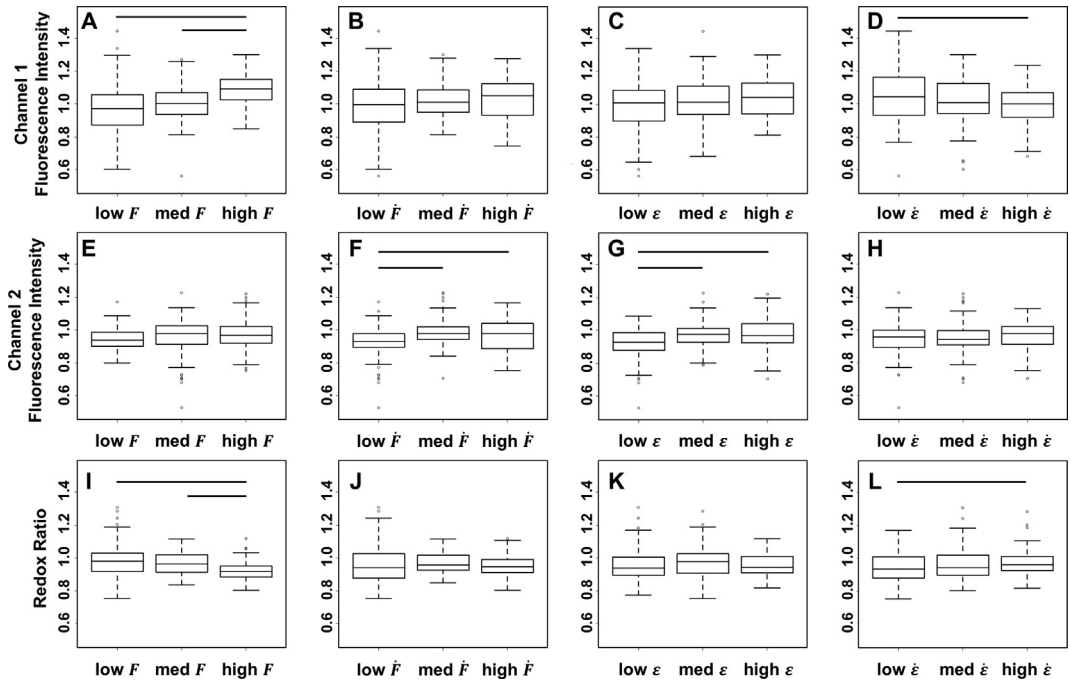

Fig. 5. Metabolic response to mechanical loading. NAD(P)H fluorescence intensity is captured by channel 1 (A–D), FAD fluorescence intensity is captured by channel 2 (E–H) and redox ratio (I–L) is calculated as [FAD]/[NAD(P)H + FAD]. Metabolic output is displayed as a function of force (A, E, F), force rate (B, F, J), strain (C, G, K) and strain rate (D, H, L). Fluorescence intensities were normalized to baseline values averaged within each sample (per mechanical bin: $n = 75$–107 images from 12 to 21 samples representing 10 animals). Significance bars = $P \leq 0.05$.

that applied in the current study could have functional consequences on cell signaling and gene expression without necessarily demonstrating a shift in biological phenotype[54]. Such downstream effects have not yet been studied using the current imaging technique in cartilage.

Though optical redox imaging overcomes many challenges associated with current metabolic analyses, this technique does not come without limitations. Testing conditions differed from physiological joint conditions such that we cannot completely rule out differential metabolic activity driven by ambient temperature, oxygen concentration, and biochemical environment in the present study. This further motivates conservative interpretation of results, as additional studies controlling for such environmental factors are warranted in order to derive mechanistic insights into truly physiological chondrocyte function. Furthermore, in addition to NAD(P)H and FAD, collagen cross-links are autofluorescent, with excitation and emission spectra that overlap with those of NAD(P)H[55]. The present study assumed consistent collagen fluorescence within and between samples because all samples were taken from animals of the same age and all metabolic images were collected when cartilage was in an unloaded state. Temperature was deemed to have no effect on collagen fluorescence in the present study, as the imaging protocol employed induced a thermal increase well below the threshold at which temperature-dependent change in collagen fluorescence becomes a concern (Supplementary Fig. S1)[56]. Future studies including more variable tissue sources, particularly those of varied maturity, or significant temperature variation should seek to account for the contribution of collagen fluorescence in the NAD(P)H channel. Similarly, while the present study assumed equal cell counts across samples, future studies including samples of varying ages and/or depth-wise analysis should account for variance in cellularity across these parameters. Additionally, preliminary data demonstrated the presence of a photobleaching effect on NAD(P)H when samples were imaged multiple times at the same location. This finding tailored the design of the present study, which imaged regionally-grouped locations without re-imaging tissue that had already been exposed to fluorescent light. Previous studies have confirmed that NADH is subject to photobleaching and have elucidated the possibility of redox flux as a biological consequence of this process[40,57]. Lastly, cartilage imaging in the present study was confined to the superficial zone due to restricted light penetration through the middle and deep zones, while mechanical analyses determined bulk properties. Imaging across the sample cross section and coupling fluorescence results with local mechanics would likely yield new insights into cartilage metabolism as chondrocyte response to mechanical loading varies between tissue zones[58]. The present study opted to image 4 mm diameter hemicylinders for the sake of mechanical loading; imaging thinly sliced cartilage cross sections could likely circumnavigate this limitation.

The present study demonstrated metabolic consequences of a single compressive load at varying physiological magnitudes in cartilage. The ability of optical redox imaging to detect mechanically-induced metabolic flux below the threshold of injury motivates the future application of this technique to various pathological models. Although multiphoton and confocal imaging, the modalities previously used for optical redox imaging, could reduce issues of imaging penetration and collagen fluorescence interference to some degree, the use of an epifluorescent microscope in the present study was motivated by access and mechanical adaptability. Indeed, these findings can be built upon by determining the immediate and long-term metabolic effects of alternative loading regimes such as cyclic loading or crack nucleation, and comparing load-induced metabolic flux between healthy and degrading cartilage can provide new insight into the mechanisms of OA progression. Furthermore, this is the first study, to the authors' knowledge, to describe adaptation of an epifluorescent microscope for optical redox imaging of FAD and NAD(P)H. The accessibility and simplicity of this technique is anticipated to attract

a variety of research groups as it provides a more cost effective and easier method to assess metabolic changes relative to existing techniques.

Cartilage redox imaging provides a solution to several fundamental limitations of previous methods of metabolic analysis. This novel application of an existing technique opens a host of opportunities for studying the intermediate cellular activity between external perturbation and altered gene expression in cartilage, a time frame which has historically been difficult to capture. Ultimately, optical redox imaging provides a simple yet powerful metric of chondrocyte metabolic phenotype, a benchmark with promising applications in OA research.

Author contributions

Study design (SKW, MCS, CRH), data collection and analysis (SKW, CRH), drafting and critically revising manuscript (SKW, MCS, CRH).

Conflict of interest

The authors declare no conflict of interest.

Acknowledgments

Funding from the UW-Madison VCGRE is gratefully acknowledged. Technical assistance with backplate calibration from Jack Fahy and imaging from Alexandra Ciolko is gratefully acknowledged.

Supplementary data

Supplementary data to this article can be found online at https://doi.org/10.1016/j.joca.2019.08.004.

References

1. Tchetina EV, Markova GA. Regulation of energy metabolism in the growth plate and osteoarthritic chondrocytes. Rheumatol Int 2018;1–12, https://doi.org/10.1007/s00296-018-4103-4.
2. Warburg O. On the origin of cancer cells. Science 1956;123:309–14.
3. Zheng J. Energy metabolism of cancer: glycolysis versus oxidative phosphorylation (Review). Oncol Lett 2012;4:1151–7, https://doi.org/10.3892/ol.2012.928.
4. Stambough JL, Brighton CT, Iannotti JP, Storey BT. Characterization of growth plate mitochondria. J Orthop Res 1984;2:235–46, https://doi.org/10.1002/jor.1100020304.
5. Blanco FJ, López-Armada MJ, Maneiro E. Mitochondrial dysfunction in osteoarthritis. Mitochondrion 2004;4:715–28, https://doi.org/10.1016/j.mito.2004.07.022.
6. Yang X, Chen W, Zhao X, Chen L, Li W, Ran J, *et al*. Pyruvate kinase M2 modulates the glycolysis of chondrocyte and extracellular matrix in osteoarthritis. DNA Cell Biol 2018;37:271–7, https://doi.org/10.1089/dna.2017.4048.
7. Goetz JE, Coleman MC, Fredericks DC, Petersen E, Martin JA, McKinley TO, *et al*. Time-dependent loss of mitochondrial function precedes progressive histologic cartilage degeneration in a rabbit meniscal destabilization model. J Orthop Res 2017;35:590–9, https://doi.org/10.1002/jor.23327.
8. Delco ML, Bonnevie ED, Bonassar LJ, Fortier LA. Mitochondrial dysfunction is an acute response of articular chondrocytes to mechanical injury. J Orthop Res 2017;36:739–50, https://doi.org/10.1002/jor.23651.
9. Coleman MC, Ramakrishnan PS, Brouillette MJ, Martin JA. Injurious loading of articular cartilage compromises chondrocyte respiratory function. Arthritis Rheum 2016;68:662–71, https://doi.org/10.1002/art.39460.
10. Han S-K, Wouters W, Clark A, Herzog W. Mechanically induced calcium signaling in chondrocytes in situ. J Orthop Res 2012;30:475–81, https://doi.org/10.1002/jor.21536.
11. Madden RMJ, Han S-K, Herzog W. The effect of compressive loading magnitude on in situ chondrocyte calcium signaling. Biomechanics Model Mechanobiol 2015;14:135–42, https://doi.org/10.1007/s10237-014-0594-4.
12. Zignego DL, Hilmer JK, June RK. Mechanotransduction in primary human osteoarthritic chondrocytes is mediated by metabolism of energy, lipids, and amino acids. J Biomech 2015;48:4253–61, https://doi.org/10.1016/j.jbiomech.2015.10.038.
13. Jutila AA, Zignego DL, Hwang BK, Hilmer JK, Hamerly T, Minor CA, *et al*. Candidate mediators of chondrocyte mechanotransduction via targeted and untargeted metabolomic measurments. Arch Biochem Biophys 2014;545:116–23, https://doi.org/10.1007/s10439-014-1183-5.
14. Jutila AA, Zignego DL, Schell WJ, June RK. Encapsulation of chondrocytes in high-stiffness agarose microenvironments for in vitro modeling of osteoarthritis mechanotransduction. Ann Biomed Eng 2014;43:1132–44, https://doi.org/10.1007/s10439-014-1183-5.
15. Adams SB, Setton LA, Kensicki E, Bolognesi MP, Toth AP, Nettles DL. Global metabolic profiling of human osteoarthritic synovium. Osteoarthr Cartil 2012;20:64–7, https://doi.org/10.1016/j.joca.2011.10.010.
16. Dai J, Yu D, Wang Y, Chen Y, Sun H, Zhang X, *et al*. Kdm6b regulates cartilage development and homeostasis through anabolic metabolism. Ann Rheum Dis 2017;76:1295–303, https://doi.org/10.1136/annrheumdis-2016-210407.
17. Sanchez C, Bay-Jensen A-C, Pap T, Dvir-Ginzberg M, Quasnichka H, Barrett-Jolley R, *et al*. Chondrocyte secretome: a source of novel insights and exploratory biomarkers of osteoarthritis. Osteoarthr Cartil 2017, https://doi.org/10.1016/j.joca.2017.02.797.
18. Kahn MK, Coverdale JA, Leatherwood JL, Arnold CE, Dabareiner RA, Bradbery AN, *et al*. Age-related effects on markers of inflammation and cartilage metabolism in response to an intra-articular lipopolysaccharide challenge in horses. J Anim Sci 2017;95:671, https://doi.org/10.2527/jas.2016.1078.
19. Salinas D, Minor CA, Carlson RP, McCutchen CN, Mumey BM, June RK. Combining targeted metabolomic data with a model of glucose metabolism: toward progress in chondrocyte mechanotransduction. PLoS One 2017;12, e0168326, https://doi.org/10.1371/journal.pone.0168326.
20. Martin JA, McCabe D, Walter M, Buckwalter JA, McKinley TO. N-Acetylcysteine inhibits post-impact chondrocyte death in osteochondral explants. J Bone Joint Surgery-American 2009;91:1890–7, https://doi.org/10.2106/JBJS.H.00545.
21. Brouillette MJ, Ramakrishnan PS, Wagner VM, Sauter EE, Journot BJ, McKinley TO, *et al*. Strain-dependent oxidant release in articular cartilage originates from mitochondria. Biomechanics Model Mechanobiol 2014;13:565–72, https://doi.org/10.1007/s10237-013-0518-8.
22. Lv M, Zhou Y, Chen X, Han L, Wang L, Lu XL. Calcium signaling of in situ chondrocytes in articular cartilage under compressive loading: roles of calcium sources and cell membrane ion channels. J Orthop Res 2017, https://doi.org/10.1002/jor.23768.
23. Skala M, Ramanujam N. Multiphoton redox ratio imaging for metabolic monitoring in vivo. Methods Mol Biol 2010;594:155–62, https://doi.org/10.1007/978-1-60761-411-1_11.
24. Alhallak K, Rebello LG, Muldoon TJ, Quinn KP, Rajaram N, Peto R, *et al*. Optical redox ratio identifies metastatic potential-

dependent changes in breast cancer cell metabolism. Biomed Opt Express 2016;7:4364–74, https://doi.org/10.1364/BOE.7.004364.
25. Quinn KP, Bellas E, Fourligas N, Lee K, Kaplan DL, Georgakoudi I. Characterization of metabolic changes associated with the functional development of 3D engineered tissues by non-invasive, dynamic measurement of individual cell redox ratios. Biomaterials 2012;33:5341–8, https://doi.org/10.1016/j.biomaterials.2012.04.024.
26. Quinn KP, Sridharan GV, Hayden RS, Kaplan DL, Lee K, Georgakoudi I. Quantitative metabolic imaging using endogenous fluorescence to detect stem cell differentiation. Sci Rep 2013;3:3432, https://doi.org/10.1038/srep03432.
27. Hou J, Wright HJ, Chan N, Tran R, Razorenova OV, Potma EO, *et al*. Correlating two-photon excited fluorescence imaging of breast cancer cellular redox state with seahorse flux analysis of normalized cellular oxygen consumption. J Biomed Opt 2016;21:60503, https://doi.org/10.1117/1.JBO.21.6.060503.
28. Walsh AJ, Castellanos JA, Nagathihalli NS, Merchant NB, Skala MC. Optical imaging of drug-induced metabolism changes in murine and human pancreatic cancer organoids reveals heterogeneous drug response. Pancreas 2016;45:863–9, https://doi.org/10.1097/MPA.0000000000000543.
29. Shah AT, Heaster TM, Skala MC. Metabolic imaging of head and neck cancer organoids. PLoS One 2017;12:1–17, https://doi.org/10.1371/journal.pone.0170415.
30. Rice WL, Kaplan DL, Georgakoudi I. Two-photon microscopy for non-invasive, quantitative monitoring of stem cell differentiation. PLoS One 2010;5, e10075, https://doi.org/10.1371/journal.pone.0010075.
31. Nishida T, Kubota S, Aoyama E, Takigawa Yz M. Impaired glycolytic metabolism causes chondrocyte hypertrophy-like changes via promotion of phospho-Smad1/5/8 translocation into nucleus. Osteoarthr Cartil 2013, https://doi.org/10.1016/j.joca.2013.01.013.
32. Mobasheri A, Vannucci SJ, Bondy CA, Carter SD, Innes JF, Arteaga MF, *et al*. Glucose transport and metabolism in chondrocytes: a key to understanding chondrogenesis, skeletal development and cartilage degradation in osteoarthritis. Histol Histopathol 2002;17:1239–67, https://doi.org/10.14670/HH-17.1239.
33. Wang C, Silverman RM, Shen J, O'Keefe RJ. Distinct metabolic programs induced by TGF-β1 and BMP2 in human articular chondrocytes with osteoarthritis. J Orthop Transl 2018;12:66–73, https://doi.org/10.1016/j.jot.2017.12.004.
34. Martin JA, Martini A, Molinari A, Morgan W, Ramalingam W, Buckwalter JA, *et al*. Mitochondrial electron transport and glycolysis are coupled in articular cartilage. Osteoarthr Cartil 2012;20:323–9, https://doi.org/10.1016/j.joca.2012.01.003.
35. Schneider CA, Rasband WS, Eliceiri KW. NIH Image to ImageJ: 25 years of image analysis. Nat Methods 2012;9:671–5, https://doi.org/10.1038/nmeth.2089.
36. Adavallan K, Gurushankar K, Nazeer SS, Gohulkumar M, Jayasree RS, Krishnakumar N. Optical redox ratio using endogenous fluorescence to assess the metabolic changes associated with treatment response of bioconjugated gold nanoparticles in streptozotocin-induced diabetic rats. Laser Phys Lett 2017;14, 065901, https://doi.org/10.1088/1612-202X/aa6b21.
37. Henak CR, Bartell LR, Cohen I, Bonassar LJ. Multiscale strain as a predictor of impact-induced fissuring in articular cartilage. J Biomech Eng 2017;139, 031004, https://doi.org/10.1115/1.4034994.
38. Losada R. Savitzky-Golay Filtering. MathWorks, Inc, 2009, https://www.mathworks.com/help/signal/ref/sgolayfilt.html. Accessed May 6, 2018.
39. scatter3: 3-D scatter plot. MathWorks, Inc n.d. https://www.mathworks.com/help/matlab/ref/scatter3.html?searchHighlight=scatter3&s_tid=doc_srchtitle#btrui17-1_seealso (accessed January 23, 2019).
40. Combs CA, Balaban RS. Direct imaging of dehydrogenase activity within living cells using enzyme-dependent fluorescence recovery after photobleaching (ED-FRAP). Biophys J 2001;80:2018–28, https://doi.org/10.1016/S0006-3495(01)76172-3.
41. Wolff KJ, Ramakrishnan PS, Brouillette MJ, Journot BJ, McKinley TO, Buckwalter JA, *et al*. Mechanical stress and ATP synthesis are coupled by mitochondrial oxidants in articular cartilage. J Orthop Res 2013;31:191–6, https://doi.org/10.1002/jor.22223.
42. Sanchez-Adams J, Leddy HA, McNulty AL, O'Conor CJ, Guilak F. The mechanobiology of articular cartilage: bearing the burden of osteoarthritis. Curr Rheumatol Rep 2014;16:451, https://doi.org/10.1007/s11926-014-0451-6.
43. Aspden RM, Jeffrey JE, Burgin LV. Letter to the editor. Osteoarthr Cartil 2002;10:588–9, https://doi.org/10.1053/joca.2002.0803.
44. Vincent TL, McLean CJ, Full LE, Peston D, Saklatvala J. FGF-2 is bound to perlecan in the pericellular matrix of articular cartilage, where it acts as a chondrocyte mechanotransducer. Osteoarthr Cartil 2007;15:752–63, https://doi.org/10.1016/j.joca.2007.01.021.
45. Millward-Sadler SJ, Wright MO, Davies LW, Nuki G, Salter DM. Mechanotransduction via integrins and interleukin-4 results in altered aggrecan and matrix metalloproteinase 3 gene expression in normal, but not osteoarthritic, human articular chondrocytes. Arthritis Rheum 2000;43:2091–9, https://doi.org/10.1002/1529-0131(200009)43:9<2091::AID-ANR21>3.0.CO;2-C.
46. Párraga Quiroga JM, Wilson W, Ito K, van Donkelaar CC. The effect of loading rate on the development of early damage in articular cartilage. Biomechanics Model Mechanobiol 2017;16:263–73, https://doi.org/10.1007/s10237-016-0815-0.
47. Li LP, Herzog W. Strain-rate dependence of cartilage stiffness in unconfined compression: the role of fibril reinforcement versus tissue volume change in fluid pressurization. J Biomech 2004;37:375–82.
48. Gemmiti CV, Guldberg RE. Shear stress magnitude and duration modulates matrix composition and tensile mechanical properties in engineered cartilaginous tissue. Biotechnol Bioeng 2009;104:809–20, https://doi.org/10.1002/bit.22440.
49. Lane Smith R, Trindade MC, Ikenoue T, Mohtai M, Das P, Carter DR, *et al*. Effects of shear stress on articular chondrocyte metabolism. Biorheology 2000;37:95–107.
50. Han G, Hess C, Eriten M, Henak CR. Uncoupled poroelastic and intrinsic viscoelastic dissipation in cartilage. J Mech Behav Biomed Mater 2018;84:28–34, https://doi.org/10.1016/j.jmbbm.2018.04.024.
51. Huber M, Trattnig S, Lintner F. Anatomy, biochemistry, and physiology of articular cartilage. Investig Radiol 2000;35:573–80.
52. Sophia Fox AJ, Bedi A, Rodeo SA. The basic science of articular cartilage: structure, composition, and function. Sport Health 2009;1:461–8, https://doi.org/10.1177/1941738109350438.
53. Pfeiffer T, Schuster S, Bonhoeffer S. Cooperation and competition in the evolution of ATP-producing pathways. Science 2001;292:504–7, https://doi.org/10.1126/science.1058079.

54. Salinas D, Mumey BM, June RK. Physiological dynamic compression regulates central energy metabolism in primary human chondrocytes. Biomechanics Model Mechanobiol 2018:1–9, https://doi.org/10.1007/s10237-018-1068-x.
55. Croce AC, Bottiroli G. Autofluorescence spectroscopy and imaging: a tool for biomedical research and diagnosis. Eur J Histochem 2014;58:2461, https://doi.org/10.4081/ejh.2014.2461.
56. Menter JM. Temperature dependence of collagen fluorescence. Photochem Photobiol Sci 2006;5:403, https://doi.org/10.1039/b516429j.
57. Tiede LM, Nichols MG. Photobleaching of reduced nicotinamide adenine dinucleotide and the development of highly fluorescent lesions in rat basophilic leukemia cells during multiphoton microscopy. Photochem Photobiol 2006;82:656, https://doi.org/10.1562/2005-09-19-RA-689.
58. Vanderploeg EJ, Wilson CG, Levenston ME. Articular chondrocytes derived from distinct tissue zones differentially respond to in vitro oscillatory tensile loading. Osteoarthr Cartil 2008;16:1228–36, https://doi.org/10.1016/j.joca.2008.02.016.